Ocean Feature Extraction from SAR Quicklook Imagery using Convolutional Neural Networks

Mohammad Hashemi, Simon Fraser University, sha196@sfu.ca, Canada
Bernhard Rabus, Simon Fraser University, btrabus@sfu.ca, Canada
Susanne Lehner, DLR EOC, Susanne.Lehner@dlr.de, Germany

Abstract

Global ocean wind and wave parameters are important inputs for weather forecasting and climate modeling. Spaceborne SAR sensors are unique resources for extraction of such ocean features due to their high resolution and wide coverage. This study examines the capability of Convolutional Neural Networks (CNNs) for extracting ocean wind features from TerraSAR-X quicklook images (QL). The QL is a freely and easily available data source to train and validate the CNN against "ground truth" ocean parameters from (also freely available) buoy data. We find that despite obvious corruption of SAR backscatter calibration during the QL formation process, the CNN with QL input produce estimates of similar accuracy for the key ocean parameter of wind speed (residual mean absolute error to ground truth: 2.2 m/s) to that of established conventional wind field retrieval methods operating on calibrated backscatter. We attribute this to the CNN exploiting higher order texture information preserved in the QL to measure the wind parameters via spatial ocean features. Other ocean parameters are also reconstructed by the CNN with reasonable accuracy. A quantitative performance comparison of our CNN architecture with higher quality inputs; calibrated backscatter and complex data is underway.

1 Introduction

Global ocean wind fields are important inputs to meteorological models as well as general circulation models (GCMs) to monitor climate change. Ocean wind fields can be operationally derived from spaceborne Scatterometers (SCATs), several of which are available at about 25 kilometer resolution [1]. Cutting edge meteorological and climatological models, however, demand at least an order of magnitude higher input resolution and spaceborne Synthetic Aperture Radar (SAR) sensors can meet this demand; through its sensitivity to cm-scale roughness and movement of the ocean surface SAR is able to measure wind fields and other ocean parameters at resolutions of 100 meter or even higher [2]. Different ocean surface phenomena such as surface currents, ocean wind and sea surface temperature all affect the SAR backscatter signal in unique ways making these parameters retrievable from the signal [3]-[5].

For the wind field, conventional estimation methods usually consist of two steps. First, wind direction is retrieved from wind-induced streaks considered to be aligned with wind direction. Second, this retrieved wind direction is used to estimate wind speed from backscattered normalized radar cross section (NRCS) by using geophysical model functions (GMFs) [6], [7]. Another study [8] derives a linear law between wind speed and sigma0 (in dB) allowing wind speed to be calculated using the NRCS input, incidence angle and wind direction values. The RMS error of the estimated U10 (sea surface wind speeds at a height of 10 m) for the method derived in [8] was 2.7 $m\,s^{-1}$. In a very recent research using a semi-empirical geophysical model, an accuracy of 1.6 $m\,s^{-1}$ has been achieved for the wind speed parameter using a dataset of 168 fully calibrated polarimetric RADARSAT-2 images [9]. This higher accuracy was reached by enhancing a previous semi-empirical model from the same authors [10].

In recent years, Convolutional and Recurrent Neural Networks (CNNs), as empirical models, have surpassed the performance of conventional methods in almost all areas involving feature extraction and pattern recognition tasks [11]. CNNs help connect the input space (image space) to the output space (ground truth values) directly and with high accuracy. In addition, different levels of learnable features naturally form within the convolutional layers during the training process and can be exploited as additional information. In this work we utilize CNNs to elucidate the potential of directly relating ocean features with SAR images.

Concretely, we perform a feasibility study in which five ocean parameters, namely wind speed, gust speed, significant wave height, dominant wave period and average wave period are derived from TerraSAR-X quicklook imagery (QL) via properly trained CNNs.

The paper is organized as follows: section 2 describes the buoy data, which is used as ground truth. Likewise in this section we describe the QL data; its statistical properties and preparation as a training dataset for the CNN. In section 3, the CNN architecture and the two methods used for ocean parameter estimation and wind speed prediction are explained. In section 4, we first present results from a quality analysis of the buoy data used for training and ground

truth verification. This is followed by the results for estimating the aforementioned five ocean parameters using CNNs. Section 5 briefly discusses the implications of our results, particularly in terms of current and future achievable accuracy.

2 Datasets

Buoy data: a large network of buoys are collecting meteorological data within the world ocean with numerous meteorological studies benefitting from these data of ocean surface and near surface parameters [12]. The key characteristics of buoy data are excellent temporal continuity but spatial sparseness. The US National Data Buoy Center gathers data from buoys both in the Atlantic and Pacific Ocean. From their dataset we extracted records of over 92 buoys with standard data covering the years 2007-2017. The data includes thirteen different ocean parameters including ocean wind direction and speed, gust speed, and significant wave height.

TerraSAR-X (TSX) Quicklook data: QLs are obtained by simple boxcar averaging and down sampling (5-10 times compared to the original resolution), as well as 8-bit clipping and conversion of (originally calibrated) SAR intensity images [13], [14]. QL data are freely available through the German Aerospace Center (DLR) EOWEB website. Basic metadata such as acquisition time and near and far range incidence angles are also available with each QL.
2252 QL images were downloaded from the EOWEB website each containing one of the aforementioned selected buoys inside the QL footprint or within a 50 km perimeter of it. The downloaded QLs were visually classified into four classes: ocean only, containing some land, containing sea ice or ships, and containing phenomena such as oil slicks manifesting as unusually low backscatter.
For the present study only the open ocean class was used, leaving 1062 QLs in the dataset. These QLs were then split into 150,385 sub scenes each measuring 128x128 pixels and also satisfying the spatial criterion of the subscene center being within 50 km of a buoy location. For each of the CNN experiments involving QLs, 67 percent of the subscenes was used as training data and the rest reserved to validate the performance of the trained network. (**Figure 1**) shows an example of a QL subscene. (**Figure 2**) shows histograms that show the distribution of the QL dataset over the value spaces of five different buoy parameters.

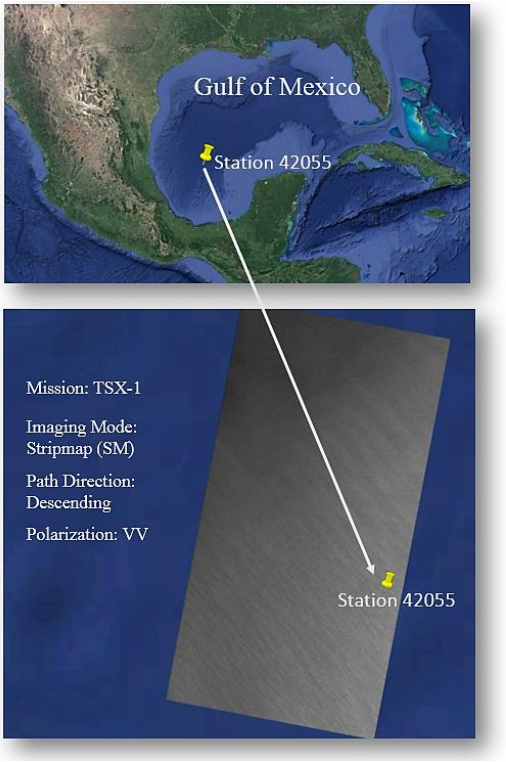

Figure 1. Example of an input image for the following CNN; TSX quicklook with size of 641×1218 within 50 kilometer of buoy ID-42055 at Gulf of Mexico.

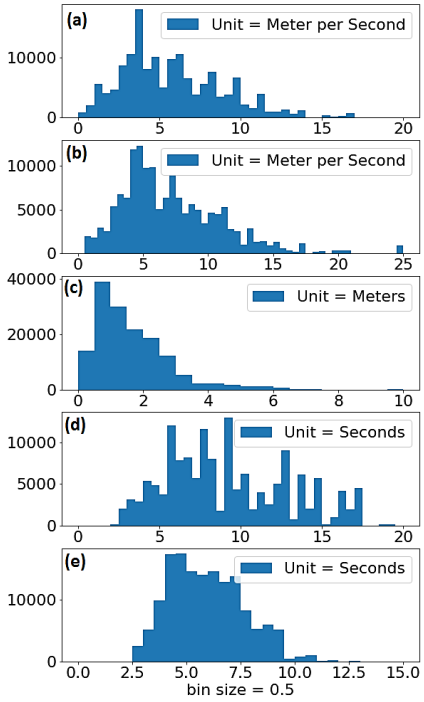

Figure 2. Histogram of QL data used for the CNN experiments, binned against different ocean parameters derived from buoy data around the QL acquisition times. Ocean parameters are; (a) Wind speed; (b) Wind gust; (c) Significant wave height; (d) Dominant wave period; (e) Average wave period.

As pre-analysis, to assess dataset suitability, we investigate basic statistical relations between the buoy data and the QL subscenes. As SAR backscatter is governed by wind excited Bragg wave and roughness of the ocean surface [2], for properly calibrated SAR data we expect high correlation coefficient between mean intensity value and wind speed. As **(Figure 3)** shows, this is clearly not the case here with the correlation coefficient between QL subscene mean intensity and buoy wind speed being very low. The significant scatter in the figure can be attributed to the process of generating the QL from SLC imagery biasing the original calibrated intensity values by shifting them to the center of the 8-bit gray scale for each QL.

The view that the scatter in **(Figure 3**) is caused by biases in the QL intensity rather than the alternate possibility of unreliable buoy wind speed data is corroborated by successful Recurrent Neural Network (RNN) experiments (presented later in section 4) that auto-predict buoy wind speed time series with reasonable accuracy. This as these experiments indirectly confirm the accuracy and spatial representativeness of the buoy measurements.

From the results of this pre-analysis (**Figure 3**) it is a-priori clear that all CNN experiments involving the QL subscenes will have to rely mainly on texture information during training process as QL intensity values will have only low training value.

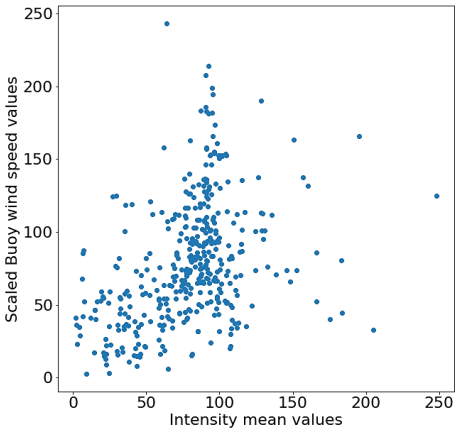

Figure 3. Correlation between mean intensity values of each QL subscene and corresponding wind speed values extracted from the buoy data.

3 Methodology

To construct a CNN architecture suitable to analyze the presented dataset and extract wind field related features from TSX QLs we choose VGG [15] as one the most successful CNN model architectures with the VGG16 model achieving a test accuracy of 92.7% in the ImageNet challenge [16]. The convolutional part of the VGG16 model structure, with weights pre-trained on ImageNet, was used as the base structure of the chosen regression network. We then replaced the fully-connected part of the VGG16 model structure with a Multi-Layer Perceptron (MLP) [17] with two hidden layers in size of 512 and 256 consecutively and a single neuron as output.

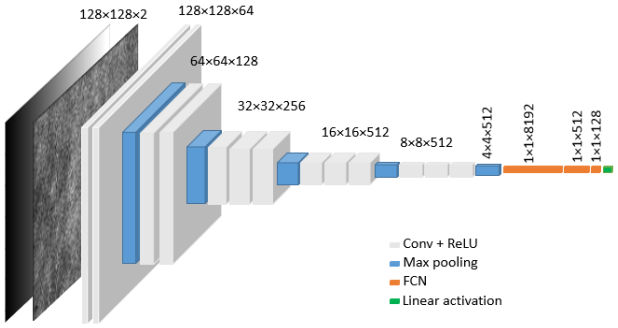

Figure 4. Structure of the Convolutional Neural Network (CNN) used for estimating the ocean parameters from the TSX Quicklook data.

The constructed CNN model architecture shown in **(Figure 4)** consists of 5 learning blocks with almost 19 million trainable parameters. "Rectified Linear Unit" (ReLU) was selected as the activation function for the hidden layers of the architecture. The output activation function for our regression model is "linear activation".

In addition, we used a Recurrent Neural Network (RNN) architecture to auto-predict wind parameters of the buoy data to assess their quality. In each case two-thirds and one-third segments of the buoy data time series were used for training and prediction, respectively. **(Figure 5)** shows the structure of the RNN used. The figure illustrates how weights from the previous state plus a new input form the new state using an iterative scheme.

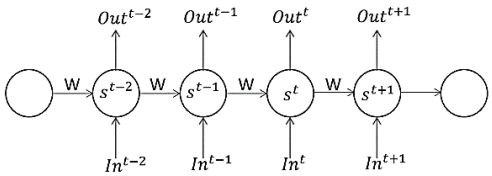

Figure 5. Structure of the Recurrent Neural Network (RNN) used for auto-prediction of buoy wind parameters to assess data quality. In^t is the input at time step t. s^t is the hidden state at time step t, which is calculated based on the previous hidden state and the current input. Out^t is the output at step t.

4 Results

RNN experiments: The ability to predict the latter portion of a time series from an earlier portion in this case is an indicator of both overall accuracy as well as (indirectly) of large-scale (~100 km) spatial representativeness of the data. **(Figure 6a, b)** shows reconstruction and prediction

results for two buoys representing diverse ocean environments: one in the Gulf of Mexico (ID-42055) in mostly calmer waters and little swell; and the other in the Atlantic Ocean (ID-44011) with higher waves and increased amount of rougher weather conditions. The time series of wind speed in each case spans the period 2007-2017, containing about 90k hourly observations.

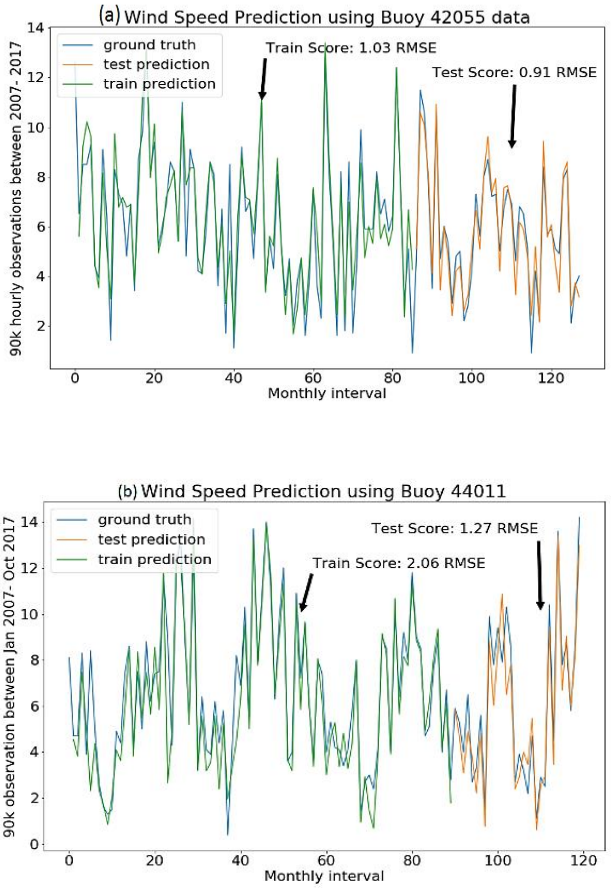

Figure 6 Auto-prediction of buoy wind speed time series (hourly observations). Period 2007-2014 is used to train the RNN; remaining period 2014-2017 is predicted Fig, **a)** ID-42055, Gulf of Mexico, RMSE=0.91 $m\ s^{-1}$ **b)** ID-44011, North Atlantic, RMSE=1.2 $m\ s^{-1}$.

For both buoys wind speed is predictable to a degree that is significant, especially for a meteorological time series. A small fraction of the records was missing and the RNN handled this robustly. These results suggest that the buoy ground truth data used for the following CNN experiments is of overall good quality and can be expected representative across the chosen QL subscene footprints.

CNN experiments: Independent CNNs were trained for five different buoy parameters ("wind speed", "gust speed", "significant wave height", "dominant wave period", "average period of all waves during a 20-minute period"). Separate CNNs were trained also for each available SAR polarization channel (HH and VV).

Training was carried out per QL subscene with the input of the CNNs consisting of two layers, the 128*128 sub-scene intensity and the corresponding incident angle map, which allowed the CNNs to decouple the local incidence angle variation from the QL intensity. Incidence angle maps were normalized globally, with respect to the overall minimum (19 degree) and maximum (45 degree) value of incidence angles in the entire data set to preserve the relative incidence range of each QL correctly.
Each network trained for 50 epochs and the reported mean absolute error values are calculated from five-fold cross validation. In the 5 fold cross validation the dataset was randomly partitioned into 5 equal size subsets, then for each run one of subsets was used for validation and the remaining four used to train the CNN. This process was repeated five times and the average accuracy reported as the final result. **(Table 1)** summarizes the mean absolute validation error for the five ocean features for the CNN experiments.

Table 1. Mean absolute estimation error (against buoy data ground truth) for five selected ocean parameters using our Convolutional Neural Network (CNN) regression model.

Polarization	VV	HH
Wind Speed	2.20 m/s	2.68 m/s
Gust speed	2.59 m/s	2.96 m/s
Significant wave height	0.79 m	0.86 m
Dominant wave period	1.47 s	3.26 s
Average wave period of all waves during the 20-minute period	0.77 s	1.14 s

5 Discussion

Probably the most important result of our study is that CNNs can retrieve ocean parameters with good accuracy **(Table 1)** from SAR quicklooks with largely destroyed backscatter calibration. The CNNs obviously rely on texture and ocean features, which consequently must contain quantitative information on the ocean parameters, e.g. there must be a unique (or most probable) structure of the ocean surface (imprinted via turbulence, depth of the atmospheric boundary layer, etc.) that corresponds to a given wind speed.
According to **(Table 1)** the accuracy of all ocean surface features are estimated with higher accuracy in VV polarization. This confirms the known fact that the VV channel is more sensitive to sea surface features than the HH channel, suggesting that texture information can be measured better in VV.
As mentioned in the introduction, state of the art methods are not able to extract ocean wind from SAR calibrated images directly. For achieving reasonable accuracy these

methods have to rely on extracting wind direction first from other sources.

The best reported RMS for ocean wind estimation to date [9] is 1.6 $m\ s^{-1}$. Considering the large input data set in [9] as well as the quality disparity between properly calibrated polarimetric full resolution image data used in [9] versus intensity biased ("uncalibrated") single polarization quicklook data used in this study, our achieved accuracy (best: 2.2 m/s for VV) holds good promise for using our CNN architecture with better quality calibrated SAR input data in the future. It should be mentioned that despite their shortcomings the freely downloadable TSX quicklooks have the highest resolution of all current SAR sensors. For TSX, making quicklooks available of the same resolution but with their calibration intact (as provided inside the TSX data products) is expected to lead already to significant further enhancement of the performance of our CNNs.

6 Conclusion

In conclusion, we have uncovered direct relationships, using a suitably constructed CNN architecture, between TSX quicklook (QL) images downloaded from DLR's EOWEB and five important ocean surface and near surface parameters specified in buoy data from the NDBC website.

We found obvious biases in the mean QL intensity apparently introduced by the QL formation process; restricting the QL to open ocean footprints was the only remediation available against this irreversible degradation of image calibration.

Despite the low quality and compromised backscatter values of the QLs the CNNs were able to extract enough higher order texture information to estimate the mentioned ocean features with reasonable to good accuracy. We consider this pilot study with low quality input data a promising stepping stone for the future extraction of ocean features from complex SAR data with related CNN architectures.

7 Literature

[1] F. M. Monaldo, and R. Beal, "Chapter 13: Wind Speed and Direction," Synthetic Aperture Radar Marine User's Manual, 305–320, 2004.

[2] J. Horstmann, W. Koch, S. Lehner, and R. Tonboe, "Wind retrieval over the ocean using synthetic aperture radar with C-band HH polarization," IEEE Transactions on Geoscience and Remote Sensing, 38(5 I), 2122–2131, 2000.

[3] WA. Qazi, W. J. Emery, and B. Fox-Kemper, "Computing ocean surface currents over the coastal California current system using 30-min-lag sequential SAR images," IEEE Transactions on Geoscience and Remote Sensing 52.12, 2014.

[4] W. Perrie, T. Xie, "Gulf Stream thermal fronts detected by synthetic aperture radar," In Proceedings of the IEEE International Geoscience & Remote Sensing Symposium, Honolulu, HI, USA, 25–30, 2010.

[5] H. Kuang, W. Perrie, T. Xie, "Retrievals of sea surface temperature fronts fromSAR imagery," J. Geophys. Res. Lett, 2012.

[6] J. Horstmann, and W. Koch, "Measurement of ocean surface winds using synthetic aperture radars," IEEE Journal of Oceanic Engineering, 30(3), 508–515, 2005.

[7] J. Schulz-Stellenfleth, and S. Lehner. "A parametric scheme for ocean wave spectra retrieval from complex synthetic aperture radar data using prior information," J. Geophys. Res, 2004.

[9] H. Fang, et al, "Ocean Wind and Current Retrievals Based on Satellite SAR Measurements in Conjunction with Buoy and HF Radar Data," Remote Sensing 9.12, 1321, 2017.

[10] T. Xie, et al, "Electromagnetic backscattering from one-dimensional drifting fractal sea surface II: Electromagnetic backscattering model," Chinese Physics B, 25.7, 074102, 2016.

[11] A. Krizhevsky, I. Sutskever, and G. E. Hinton, "Imagenet classification with deep convolutional neural networks," Advances in neural information processing systems, 2012.

[12] N. N. Soreide, C. E. Woody, and S. M. Holt, "Overview of ocean based buoys and drifters: Present applications and future needs," OCEANS, MTS/IEEE Conference and Exhibition, Vol. 4. IEEE, 2001.

[13] M. Eineder, et al, "TerraSAR-X ground segment, basic product specification document," No. TX-GS-DD-3302. CLUSTER APPLIED REMOTE SENSING (CAF) OBERPFAFFENHOFEN (GERMANY), 2008.

[14] H. Breit, et al, "TerraSAR-X SAR processing and products," IEEE Transactions on Geoscience and Remote Sensing 48.2, 727-740, 2010.

[15] K. Simonyan, and A. Zisserman, "Very deep convolutional networks for large-scale image recognition," arXiv preprint arXiv, 1409.1556, 2014.

[16] O. Russakovsky, et al, "Imagenet large scale visual recognition challenge," International Journal of Computer Vision 115.3, 211-252, 2015.

[17] D. W. Ruck, et al, "The multilayer perceptron as an approximation to a Bayes optimal discriminant function," IEEE Transactions on Neural Networks 1.4, 296-298, 1990.